JACS
JOURNAL OF THE AMERICAN CHEMICAL SOCIETY

ARTICLE

pubs.acs.org/JACS

Reconciling the Discrepancies between Crystallographic Porosity and Guest Access As Exemplified by Zn-HKUST-1

Jeremy I. Feldblyum,[†,‡] Ming Liu,[§] David W. Gidley,[*,§] and Adam J. Matzger[*,†,‡]

[†]Macromolecular Science and Engineering, [‡]Department of Chemistry, and [§]Department of Physics, University of Michigan, Ann Arbor, Michigan 48109, United States

Supporting Information

ABSTRACT:

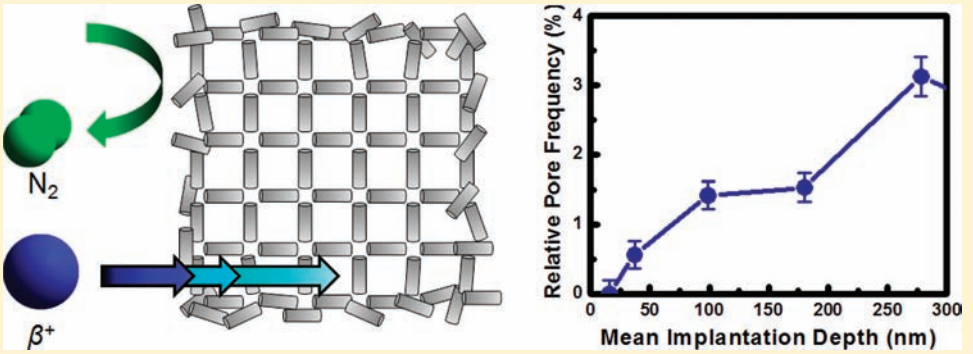

There are several compounds for which there exists a disconnect between porosity as predicted by crystallography and porosity measured by gas sorption analysis. In this paper, the Zn-based analogue of $Cu_3(btc)_2$ (HKUST-1), $Zn_3(btc)_2$ (Zn-HKUST-1; btc = 1,3,5-benzenetricarboxylate) is investigated. Conventional analysis of Zn-HKUST-1 by powder X-ray diffraction and gas sorption indicates retention of crystalline structure but negligible nitrogen uptake at 77 K. By using positron annihilation lifetime spectroscopy, a densified surface layer preventing the entry of even small molecular species into the crystal framework is revealed. The material is shown to have inherent surface instability after solvent removal, rendering it impermeable to molecular guests irrespective of handling and processing methods. This previously unobserved surface instability may provide insight into the failure of other microporous coordination polymers to exhibit significant porosity despite crystal structures indicative of regular, interconnected, microporous networks.

INTRODUCTION

The myriad and tunable chemistries and pore structures of microporous coordination polymers (MCPs) have significantly expanded the potential capabilities of porous materials.[1] MCPs have shown great promise for applications such as gas separation[2] and storage,[3] catalysis,[4] and selective adsorption from the liquid phase.[5] However, for many MCPs there is a discrepancy between the theoretical surface area predicted by crystallographic considerations and experimentally determined porosity.[6−8] Although underperformance in MCPs has been attributed to interpenetration,[9] incomplete removal of guests from pores,[10] and pore collapse,[11] and various methodologies have been employed to achieve higher porosity,[11,12] direct detection and analysis of these failure modes remains difficult and can yield ambiguous results. The structural purity of MCPs is most often analyzed by X-ray diffraction and gas sorption techniques. Powder X-ray diffraction (PXRD) can yield information about crystallinity but is less well suited for examining disorder. Gas sorption techniques provide quantitative measurements of accessible internal surface area but are subject to kinetic limitations and do not probe closed pores.

In this study, we describe investigations on an MCP that, despite promising structural data, fails to yield substantial gas uptake by conventional gas sorption techniques. A strategy for improving the performance of MCPs for specific applications is the discovery and employment of isostructural analogues where one metal is replaced with another or different metals are mixed in the same structure.[13] Lighter metals can be used in this manner to improve surface area,[14−16] and selection of metal can be used to enhance and control catalytic and photocatalytic activity.[17,18] $Cu_3(btc)_2$ (commonly "HKUST-1", hereafter "Cu-HKUST-1", Figure 1) was one of the first MCPs demonstrated to retain its crystal structure and exhibit permanent porosity upon removal of guest molecules.[19] In addition, it is one of the few commercially marketed MCPs,[20] and a great deal of effort has been spent on making it an industrially viable and useful material.[21−24] The prevalence of zinc paddlewheels[25] in a variety of MCPs suggests that zinc is a promising metal with which to construct an isostructural analogue to Cu-HKUST-1 ($Zn_3(btc)_2$, hereafter

Received: June 16, 2011
Published: October 19, 2011

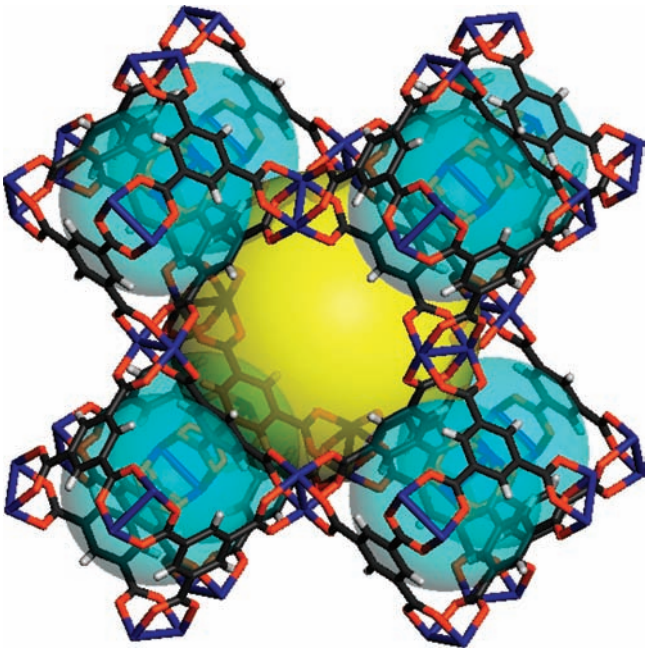

Figure 1. HKUST-1 structure as viewed down the [100] direction, angled slightly to show three-dimensional structure (Cu, blue; C, black; O, red; H, light gray). The void spaces of the large and small pores present within the structure are depicted by yellow and blue spheres, respectively.

"Zn-HKUST-1"); however, zinc paddlewheel MCPs frequently exhibit lower-than-expected surface areas or complete collapse upon removal of axial ligands.[26,27] Although the failure of these materials to exhibit theoretically achievable porosity has not been explored in detail, their underperformance may be due to structural rearrangement or distortion of the zinc paddlewheel under dry conditions.[28,29] Although Zn-HKUST-1 was synthesized previously,[30] no evidence of permanent porosity was reported.

Our group recently applied positron annihilation lifetime spectroscopy (PALS)[31,32] to investigate the porosity, thermal stability, and CO_2 gas adsorption of the prototypical MCP MOF-5.[33] Positron interaction with dielectric materials can form positronium, the atom-like bound state of a positron and an electron. The electron and positron comprising a positronium atom can have either parallel or antiparallel spins. The species with parallel spins, orthopositronium (Ps), has a characteristic lifetime in vacuum of 142 ns. In a porous dielectric material, the lifetime of Ps is reduced in a manner directly related to the size of pores within that material. By bombarding a sample with positrons and detecting γ rays emitted from Ps decay, a Ps lifetime (or a distribution of lifetimes) can be determined and correlated to a precise pore size (or pore size distribution) for the analyzed material. PALS has inherent advantages over gas sorption techniques as an analytical tool to study porous materials. Most importantly, an accessible, interconnected pore space is not required to yield pore size and occurrence data, as energetic positrons will pass directly through insulating material until losing enough energy to form positronium or annihilate directly via positron−electron interaction.[31] In addition, by tuning the energy of implanted positrons, the bulk and surface of a material can be studied separately.

Using a combination of PXRD, gas sorption analysis, PALS, depth-profiled PALS, optical microscopy, and NMR spectroscopy, a thorough analysis of the failure mode of Zn-HKUST-1 is

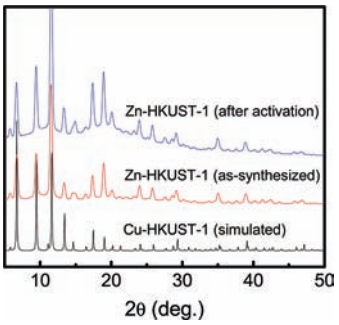

Figure 2. Powder X-ray diffractograms of Zn-HKUST-1 immediately after synthesis and after evacuation under reduced pressure (~20 mTorr) compared with simulated diffractogram of Cu-HKUST-1.

provided. Crystallinity after evacuation is maintained, yet no observable porosity is found by gas sorption analysis. PALS provides an explanation for these results and is able to demonstrate that the surface of Zn-HKUST-1 is unstable after drying.

RESULTS AND DISCUSSION

The crystallinity of Zn-HKUST-1 was probed by PXRD (Figure 2) immediately after crystal growth and after evacuation under reduced pressure (~20 mTorr). Zn-HKUST-1 appears isostructural to Cu-HKUST-1, with a slightly larger unit cell (Cu-HKUST-1, $a = 26.343 \pm 0.005$ Å;[19] Zn-HKUST-1, $a = 26.520 \pm 0.001$ Å). Differences in peak intensities between simulated and experimental diffractograms can be attributed to coordinated guest molecules. Such differences in peak intensity have previously been attributed to pore occlusion by molecular guests.[9] Despite retention of crystallinity after attempted activation, no condition was found for which Zn-HKUST-1 exhibited significant porosity by N_2 adsorption surface area measurements. Attempted activation methods included evacuation both at room temperature and at 170 °C, use of DMF, $CHCl_3$, and benzene[11] as activation solvents, activation by flowing dry nitrogen at atmospheric pressure, and activation using supercritical CO_2.[12] Furthermore, attempts at accessing the pores of dry Zn-HKUST-1 crystals by adsorption of Ar at 87 K or CO_2 at 298 K yielded no indication of porosity in the material (representative isotherms provided in Figure S1 of the Supporting Information).

Reasonable hypotheses for the failure of Zn-HKUST-1 to exhibit porosity include complete or partial structural collapse upon drying, interpenetration, an inability to remove molecular guests trapped in the framework, and/or the presence of a surface layer[34,35] blocking entry of gases into the crystal. PXRD data (Figure 2) were used to rule out complete structural collapse. Computational modeling of a hypothetical interpenetrated material having the framework structure of Cu-HKUST-1 (HKUST-1_int) showed that interpenetration was unlikely due to steric hindrance between interpenetrating structures (Figure S2). Furthermore, a simulated powder X-ray diffractogram of HKUST-1_int lacked peaks at 6.7° and 11.55° that are present in the simulated and experimentally determined powder X-ray diffractograms of Cu-HKUST-1 and Zn-HKUST-1 (Figure S3). Upon ^{1}H NMR analysis of Zn-HKUST-1 dried under dynamic vacuum at 170 °C (see Experimental Methods), DMF was found to be present at a ratio of 2.19:1 DMF:BTC (Figure S4). The NMR data corroborate the sorption data that indicate a closed structure but cannot be used to rule out one or another hypothesis, as DMF might reasonably be

found trapped in the MCP framework, considering any of the failure models enumerated above.

Given its proven utility in probing buried pores[32] and MCP pore systems,[33] PALS was used to determine whether empty pores remained within activated Zn-HKUST-1 crystals. Ps annihilation lifetimes were determined by fitting the raw lifetime data (Figure 3) to multiple, superimposed exponential decays. Two separate Ps decay components were found, corresponding to lifetimes of 2.13 ± 0.13 and 5.24 ± 0.17 ns, as would be expected were Ps trapped in either the small or the large pores present in the Zn-HKUST-1 crystal structure (Figure 1). The fitting of these two distinct lifetimes indicates that Ps does not freely diffuse through the Zn-HKUST-1 pore space because a freely diffusing Ps atom would sample all voids, and thus only a single average Ps lifetime would be fit in the spectrum (beam PALS results below will confirm this claim of trapping). Using quantum mechanical models[36−39] to correlate calculated lifetimes to pore sizes, pore diameters of 0.59 ± 0.02 and 0.97 ± 0.02 nm were deduced. Pore sizes were determined from the crystal structure using the diameters of the inscribed sphere (Figure 1) of each pore (taking into account neutral van der Waals radii of relevant atoms at the pore walls). Idealized pore sizes for the small and large pores determined in this manner are 0.56 and 1.10 nm, respectively, in good agreement with PALS-derived values. The fractional contributions from each lifetime component, provided as intensities relative to the total number of all positrons emitted from the ^{22}Na source, were 5.1 ± 0.2% and 4.5 ± 0.3% for the small and large pores, respectively. (Note that since in our PALS apparatus only half the positrons from the ^{22}Na source can stop in the sample, these intensities should be doubled when comparing with beam PALS results below.) In the ideal crystal structure, the number of small pores is equal to the number of large pores. However, the larger pores, having nearly 4 times the surface area and 8 times the volume of the smaller pores, will preferentially trap positronium. Hence, these initial PALS data hint at a deficit in the number of empty large pores compared with that expected from the ideal Zn-HKUST-1 crystal structure. For a pristine crystal, an intensity significantly greater than 5.1% would be expected for the large-pore annihilation component. The depth dependence of this deviation is explored and discussed below. The small apertures between large and small pores, possibly constricted further by the presence of residual solvent (as evidenced by NMR), may account for Ps trapping in individual voids. As such Ps trapping on time scales of 5−10 ns does not rule out gas uptake into interconnected 1 nm voids on a time scale 10^9 times longer, these data solely demonstrate the presence of empty pores generally consistent with the crystallographic structure of Zn-HKUST-1.

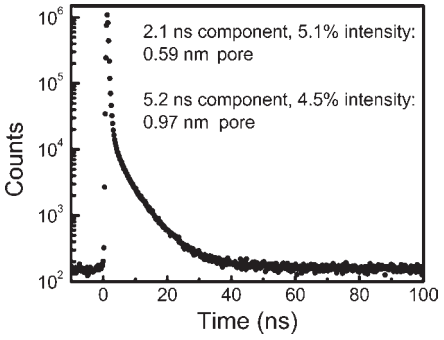

Figure 3. PALS spectrum of Zn-HKUST-1 after evacuation under reduced pressure (~20 mTorr). Lifetimes, relative intensities, and corresponding cubic pore lengths are provided.

As experimental PALS data describe a structure in which at least a significant fraction of pores in the *bulk* are present and accessible by positrons and Ps, depth-profiled beam PALS[32] was used to examine the pore structure at the surface of Zn-HKUST-1. By moderating the energy of positrons directed toward the sample, the positrons' mean implantation depth, and hence, the depth of Ps formation, was controlled. The depth profiling results (Figure 4) are very revealing. First, no Ps diffuses through interconnected pores back to the sample surface, where it would escape into vacuum. This is consistent with Ps trapping in the pores and/or with pores sealed at the surface to prevent any escape. Additionally, fitting the lifetime spectrum at each implantation depth requires two Ps lifetimes corresponding to two pore sizes similar to those found by bulk fitting (Figure 4a), for which the intensity of Ps annihilating in the larger pore is a factor of 5 lower in the region within 500 nm of the crystal surface than in the bulk (Figure 4b). At the shallowest mean implantation depth (16 nm), there is *virtually no Ps annihilation in the larger pores*. Throughout the surface region, the intensity of Ps annihilating in the larger pores gradually increases with depth but is still much lower than that in the bulk of the crystal. Moreover, the top 30−40 nm may be largely devoid of the larger pores due to complete collapse of the structure, leaving only microvoids from

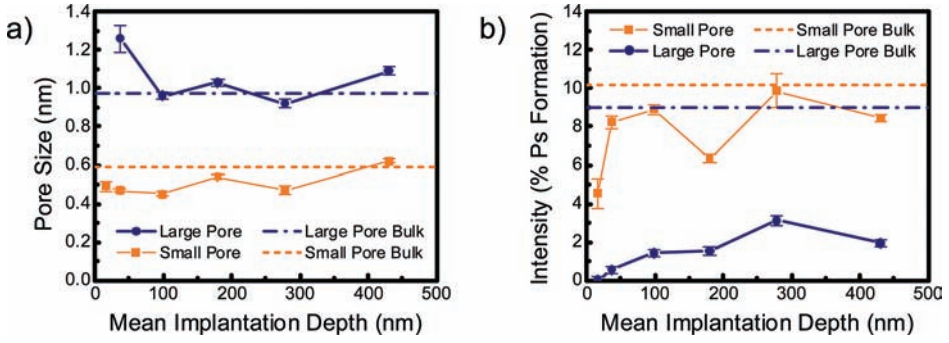

Figure 4. Beam PALS of Zn-HKUST-1 after evacuation under reduced pressure (~20 mTorr) showing (a) pore size and (b) annihilation intensity at controlled depths. Two pores were detected corresponding to the small and large pores expected from the Zn-HKUST-1 crystal structure. Values obtained at room temperature for small (dotted line) and large (dash-dotted line) pores by PALS measurements of crystal bulk from Figure 3 are shown for reference. Note that reference intensity values are doubled to account for differences in sample holder positioning between bulk and beam measurements. As no large-pore component was detected at the shallowest depth (16 nm), no pore size was obtainable.

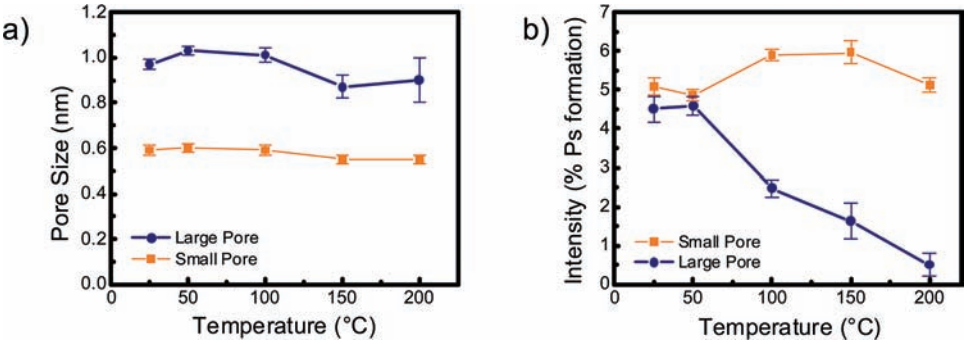

Figure 5. PALS measurements of small and large pores of Zn-HKUST-1 at room temperature (~25 °C) and after successive 30 min heating/cooling cycles at temperatures up to 200 °C. (a) Pore size and (b) annihilation intensity of small pores remains largely unchanged, but large-pore intensity vanishes as temperature increases.

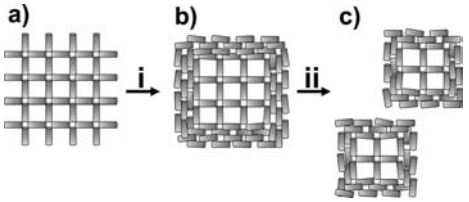

Figure 6. Schematic representation of material failure of Zn-HKUST-1. (a) Solvent-filled material is open to guest exchange. After drying under vacuum (i), (b) the surface of Zn-HKUST-1 collapses, leaving only small pores at the surface. Mechanically grinding the material into a fine powder (ii) leads to (c) surface collapse of smaller Zn-HKUST-1 fragments.

debris (as a result, the fitted values of the short and long Ps lifetimes could well deviate from those of the bulk crystal). This clearly indicates that the surface of the Zn-HKUST-1 crystal is densified, presumably due to pore collapse. As the large pores are necessary for interconnection between all pore space within the framework, a blocking or complete collapse of large pores at the surface effectively inhibits the ability of adsorbates such as N_2 gas from entering the bulk structure.

To further explore the instability of the large pores in Zn-HKUST-1, a bulk sample was heated to 50 °C for 30 min, cooled to room temperature, and subsequently analyzed by PALS (Figure 5). This procedure was then repeated on the same sample at 100, 150, and 200 °C. After the initial period of heating, the pore characteristics remained largely unchanged. However, at 100 °C, the intensity of Ps annihilation in the large pores dropped by a factor of about 2 to 2.47 ± 0.23%, and on further heating at higher temperatures, Ps annihilation in the large pores dropped to 0.51 ± 0.29%, accounting for only a small fraction of the open pore space left in the material (Figure 5b). At higher temperatures, a concomitant decrease in the size of the large pores was observed (Figure 5a). In contrast, the intensities and pore sizes of the small pores showed little change over successive heating and cooling cycles. The slight increase in Ps annihilation intensity in the small pores at higher temperatures can be attributed to reduced Ps formation in large pores, limiting annihilation to the small pores of the material. Both the reduced occurrence and reduced pore size indicate collapse solely of the larger pores after heating at higher temperatures. These trends are consistent with degradation of the bulk material and indicate that the larger pores responsible for gas transport exhibit comparatively poorer

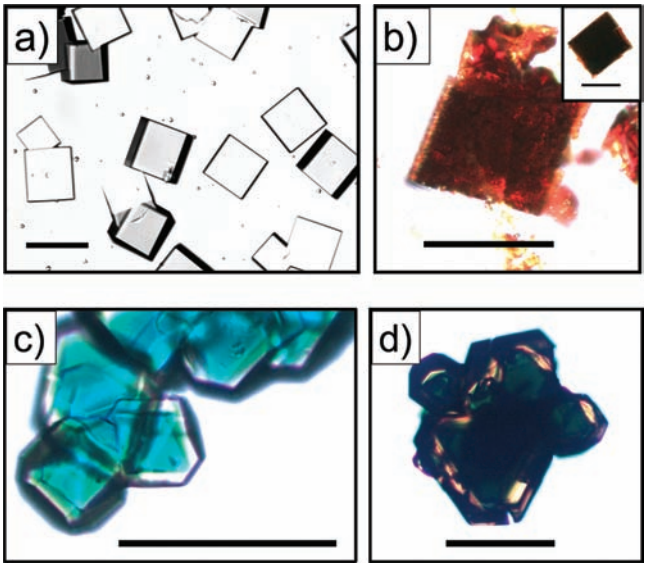

Figure 7. (a) Optical micrograph of Zn-HKUST-1 examined immediately after crystallization. (b) Optical micrograph of a cross section of Zn-HKUST-1 after immersion in saturated iodine/$CHCl_3$ solution for 7 days. Inset: crystal before cross section. (c) Optical micrograph of Zn-HKUST-1@Cu-HKUST-1. (d) Optical micrograph of Zn-HKUST-1@Cu-HKUST-1 after immersion in saturated iodine/$CHCl_3$ for 24 h. Scale bars, 100 μm.

durability. Presumably, the surface of the crystal is even less durable to pore collapse than the interior, even without heating.

After the nature of structural failure in Zn-HKUST-1 was confirmed, a sample of activated Zn-HKUST-1 was mechanically crushed under a nitrogen atmosphere to determine whether the surface layer was due to the presence of dense guest-filled layer or collapse of the crystal itself. No porosity was observed by measuring N_2 uptake (Figure S5) of the crushed Zn-HKUST-1 at 77 K, indicating that the surface collapse is apparently due to inherent instability of the dry material (Figure 6). This instability suggests that further attempts at activation, barring postsynthetic chemical modification, are unlikely to yield a dry, stable, porous material.

Although the surface of Zn-HKUST-1 appears to be unstable, highly ordered crystals grow to sizes of up to 100 μm when solvothermally synthesized in DMF (Figure 7a). To examine

whether molecular guests could enter the pores of Zn-HKUST-1 in solvent, MCP crystals were immersed in saturated solutions of strongly colored species including Nile red, methylene blue, azobenzene, and elemental iodine. Only iodine was found to diffuse slowly into Zn-HKUST-1 crystals, as evidenced by a color change from colorless to dark orange-brown over a period of 7 days (Figure 7b). The small pore aperture of the larger pores (0.66 nm after complete removal of axially coordinated ligands) precluded adsorption of the organic dyes. The lack of organic dye uptake also eliminates the possibility that iodine uptake was due to mesopore or macropore defects. To examine the diffusion of iodine in the HKUST-1 structure further, a layer of Zn-HKUST-1 was grown on crystals of Cu-HKUST-1 in a core−shell configuration[40,41] (Zn-HKUST-1@Cu-HKUST-1, Figure 7c, Figure S7). Such a configuration provided a more rapid means to confirm the diffusion of iodine into the crystal due to the strong color contrast between iodine in $CHCl_3$ and Cu-HKUST-1. After immersion in saturated iodine/$CHCl_3$ for a single day, substantial diffusion of iodine into the copper portion of Zn-HKUST-1@Cu-HKUST-1 was observed (Figure 7d). These results show that, in solution, both bulk Zn-HKUST-1 crystals and Zn-HKUST-1 shells bound to Cu-HKUST-1 cores are stable and exhibit accessible, interconnected pore space before the removal of solvents. In contrast, crystals of Zn-HKUST-1 soaked in saturated iodine/$CHCl_3$ after evacuation exhibited no observable iodine uptake after 7 days (Figure S8). This behavior is consistent with the other observations in this study, suggesting that, after surface densification on evacuation, reimmersion of Zn-HKUST-1 in solvent does not restabilize the surface or open it to guest inclusion.

CONCLUSIONS

A detailed description of the mode of failure in the MCP Zn-HKUST-1 has been presented. Retention of crystallinity after activation juxtaposed with a demonstrated lack of accessible porosity can be explained by combining bulk and depth-profiled PALS data. Analysis by these techniques reveals the preservation of an ordered and open pore network in the bulk of the Zn-HKUST-1 crystals made inaccessible by a densified layer at the surface. The instability of the Zn-HKUST-1 surface was shown to be characteristic of the material in dry environments, as dry, crushed crystals exhibited no significant uptake of N_2 gas despite an interior shown to have open pore space. In contrast, the material exhibited accessible porosity before removal of solvent by the infusion of iodine both throughout bulk Zn-HKUST-1 crystals and through Zn-HKUST-1 layers encapsulating Cu-HKUST-1 crystals immersed in $CHCl_3$.

These results deepen the understanding of a previously unknown[42] mode of failure in MCPs and suggest that a lack of observable gas uptake in dried crystals should not be taken as conclusive evidence for complete structural collapse or pore filling by guests. Although some MCPs may require specialized activation techniques[11,12] to maintain stability in the dry state, it has been shown that instability of specific structural features (for example, the largest pores) within an MCP may fundamentally limit porosity for solvent-free applications. Porous materials exhibiting a lack of accessible internal surface area after solvent removal may still be useful for liquid-phase adsorption applications,[43−45] where pores may remain open and interconnected.

EXPERIMENTAL METHODS

Synthesis of $Zn_3(btc)_2$ (Zn-HKUST-1). A mixture of 1,3,5-benzene tricarboxylic acid (H_3BTC, 39.5 mg, 0.188 mmol, Acros Organics) and $Zn(NO_3)_2 \cdot 6H_2O$ (170.7 mg, 0.574 mmol, Fisher Scientific) was dissolved in 10 mL *N*,*N*-dimethylformamide (DMF, Fisher Scientific), aided by sonication. The resultant solution was filtered through P5 filter paper (Fisher Scientific) into a 20 mL scintillation vial and subsequently incubated at 85 °C for ∼16 h. Incubation yielded colorless, transparent cubic crystals. Note that longer incubation times yielded opaque white crystals exhibiting poorer crystallinity when analyzed by PXRD. After incubation, solvent was decanted and replaced with ∼10 mL pure DMF three times. The solvent was then decanted and replaced with chloroform four times over the next 48 h, during which the sample was stored in a tightly capped vial in a desiccator. The sample was then held under dynamic vacuum (20 mTorr) at room temperature for ∼10 h and transferred to a N_2 glovebox for storage and further analysis.

Synthesis of Zn-HKUST-1@Cu-HKUST-1. First, 5 mL of >18.2 MΩ cm^{-1} H_2O, 5 mL of ethanol (Decon Labs), and 5 mL of DMF were added to a mixture of 0.30 g of H_3BTC (1.43 mmol) and 0.60 g of $Cu(NO_3)_2 \cdot 2.5H_2O$ (2.58 mmol, Fisher Scientific) in a 20 mL scintillation vial. The resultant solution was sonicated until it became a uniform cloudy blue color (∼5 min). Concentrated HCl was then added dropwise until the solution became a transparent blue (∼12 drops from a glass pipet). The clear solution was incubated at 85 °C for ∼20 h, after which a thick layer of blue Cu-HKUST-1 crystals formed at the bottom of the vial. The vial was removed and allowed to cool to room temperature. The solvent was subsequently decanted and replaced three times with ∼10 mL of fresh DMF.

In a separate 20 mL scintillation vial, a precursor solution of Zn-HKUST-1 was prepared by adding 0.228 g of $Zn(NO_3)_2 \cdot 6H_2O$ (0.765 mmol), 0.0526 g of H_3BTC (0.250 mmol), and 10 mL of DMF and sonicating until complete dissolution of the solid. The solvent from the vial containing the Cu-HKUST-1 was decanted and replaced with the Zn-HKUST-1 precursor solution. The crystals in the precursor solution were incubated at 85 °C for ∼20 h and subsequently cooled to room temperature. The solvent was immediately exchanged three times with pure DMF and analyzed by PXRD. Upon further examination by optical microscopy, a heterogeneous mixture of Cu-HKUST-1 and Zn-HKUST-1@Cu-HKUST-1 was observed.

Infusion of Iodine in Zn-HKUST-1 and Zn-HKUST-1@Cu-HKUST-1. Zn-HKUST-1 was synthesized in DMF as described above. After crystals formed, the solvent was decanted and replaced with ∼10 mL of pure DMF three times. The solvent was then decanted and replaced with chloroform, after which crystals were analyzed by PXRD. Crystals were then transferred to a 4 mL vial containing a minimum amount of chloroform (∼0.5 mL) to keep samples submerged for 1 week. Elemental iodine (Fisher Scientific) was added liberally until the solution reached saturation. The vial containing Zn-HKUST-1, solvated iodine, and solid iodine was placed on a shaker (IKA KS 260) and agitated at 120 rpm for 7 days. Crystals were then analyzed by PXRD and optical microscopy. To visualize cross sections, a single crystal was isolated and carefully sliced on opposite sides with a razor to obtain a cross section from the center of the crystal (Figure 7). Crystals of Zn-HKUST-1@Cu-HKUST-1 were synthesized as described above. The sample was then treated similarly as described for Zn-HKUST-1, but immersion in saturated iodine/$CHCl_3$ was limited to 24 h. Crystals of Zn-HKUST-1 after evacuation were transferred from a N_2 glovebox into a vial containing chloroform under ambient atmosphere. These crystals were soaked in saturated iodine for 7 days and imaged as described above.

Positron Annihilation Lifetime Spectroscopy. Dry sample was loaded in a N_2 glovebox into a well-type sample holder with a 4 μCi ^{22}Na positron source deposited on the bottom of the well. The sample holder was placed between two plastic scintillators to detect γ rays signaling positron emission from the ^{22}Na source and subsequent Ps

annihilation. Before measurement of Ps lifetimes within the sample, the sample holder was evacuated to 10 mTorr to eliminate significant interaction between Ps and residual gas. A histogram of the lifetimes of discrete annihilation events was obtained at a rate of 60 counts s^{-1} (representative histogram in Figure 3). Pore sizes were determined from lifetime data with an extended Tao-Eldrup model[36−39] using in-house software. Samples remained in the PALS apparatus under dynamic vacuum (10^{-3} Torr) during sample heating and cooling, and measurements of heated samples were taken at room temperature after heating and subsequent cooling.

Depth-Profiled Positron Annihilation Lifetime Spectroscopy. An optically thick layer of analyte was deposited on a piece of conductive tape attached to a sample holder. The sample holder was inserted into a depth-profiled PALS apparatus, in which monoenergetic positrons are focused on the sample under high-vacuum conditions.[32] The energy of positrons impinging upon the sample was varied between 1 and 6 keV, controlling the depth at which Ps formed and annihilated within the sample. In this manner, information regarding pore size and relative porosity was obtained, as well as information about the ability of Ps to diffuse out of the structure before annihilation.

Surface Area Determination by N_2 Gas Sorption. Volumetric N_2 sorption isotherms were obtained on a Quantachrome NOVA 4200e, using 99.999% purity N_2 (Cryogenic Gases). Samples (∼30 mg) were transferred to sample cells in a N_2 glovebox and rapidly attached to the surface area analyzer to avoid exposure to air. Sample cells were immediately subject to dynamic vacuum, after which surface area analysis was performed.

Determination of CO_2 and Ar Gas Sorption. Volumetric CO_2 and Ar isotherms were obtained on a Quantachrome Autosorb-1C at room temperature and 87 K, respectively. Samples were treated identically as in N_2 gas sorption experiments described above. Gases used were of 99.999% purity (Cryogenic Gases).

Powder X-ray Diffraction Analysis. Analyte crystals were coated in Paratone N oil (Hampton Research), mounted on a Nylon loop, and placed in a goniometer head. Samples were then analyzed with a Rigaku R-Axis Spider diffractometer equipped with a Cu Kα X-ray source (λ = 1.5406 Å) operating at 50 kV and 40 mA. An image plate detector was used to collect images in 10 min scans by transmission with χ = 45°, ϕ rotating at 10°/min, and ω oscillating between 80° and 140°. Integration of images was carried out using the AreaMax 2.0 software package with a step size of 0.2° in 2θ.

^{1}H Nuclear Magnetic Resonance Spectroscopy. Crystals of Zn-HKUST-1 were synthesized and washed with DMF and chloroform as described above. The Zn-HKUST-1 was then dried under dynamic vacuum (∼20 mTorr) at 170 °C for ∼10 h. After sorption analysis, the crystals were transferred rapidly from a nitrogen glovebox atmosphere to a 1 M solution of NaOD in D_2O. The solution was agitated for ∼5 min, after which time the crystals were completely dissolved. The resultant solution was characterized by ^{1}H NMR spectroscopy.

■ ASSOCIATED CONTENT

Supporting Information. N_2, Ar, and CO_2 isotherms, computational modeling, NMR and PXRD data, and optical micrograph of Zn-HKUST-1. This material is available free of charge via the Internet at http://pubs.acs.org.

■ AUTHOR INFORMATION

Corresponding Author
gidley@umich.edu; matzger@umich.edu

■ ACKNOWLEDGMENT

This work is supported by the National Science Foundation (DMR-0907369). J.I.F. gratefully acknowledges support from the National Science Foundation Graduate Research Fellowship Program (NSF-GRFP). We thank Dr. William E. Frieze for the code to acquire and analyze PALS and depth-profiled beam PALS data, Dr. Jennifer K. Schnobrich for supercritical CO_2 activation, and Dr. Antek G. Wong-Foy for technical advice and helpful discussions.

■ REFERENCES

(1) Férey, G. *Chem. Soc. Rev.* **2008**, *37*, 191.
(2) Li, J. R.; Kuppler, R. J.; Zhou, H.-C. *Chem. Soc. Rev.* **2009**, *38*, 1477.
(3) Murray, L. J.; Dincă, M.; Long, J. R. *Chem. Soc. Rev.* **2009**, *38*, 1294.
(4) Lee, J.; Farha, O. K.; Roberts, J.; Scheidt, K. A.; Nguyen, S. T.; Hupp, J. T. *Chem. Soc. Rev.* **2009**, *38*, 1450.
(5) Cychosz, K. A.; Ahmad, R.; Matzger, A. J. *Chem. Sci.* **2010**, *1*, 293.
(6) Walton, K. S.; Snurr, R. Q. *J. Am. Chem. Soc.* **2007**, *129*, 8552.
(7) Düren, T.; Bae, Y. S.; Snurr, R. Q. *Chem. Soc. Rev.* **2009**, *38*, 1237.
(8) Schnobrich, J. K.; Koh, K.; Sura, K. N.; Matzger, A. J. *Langmuir* **2010**, *26*, 5808.
(9) Hafizovic, J.; Bjørgen, M.; Olsbye, U.; Dietzel, P. D. C.; Bordiga, S.; Prestipino, C.; Lamberti, C.; Lillerud, K. P. *J. Am. Chem. Soc.* **2007**, *129*, 3612.
(10) Barthelet, K.; Marrot, J.; Férey, G.; Riou, D. *Chem. Commun.* **2004**, 520.
(11) Ma, L. Q.; Jin, A.; Xie, Z. G.; Lin, W. B. *Angew. Chem., Int. Ed.* **2009**, *48*, 9905.
(12) Nelson, A. P.; Farha, O. K.; Mulfort, K. L.; Hupp, J. T. *J. Am. Chem. Soc.* **2009**, *131*, 458.
(13) Lim, C. S.; Schnobrich, J. K.; Wong-Foy, A. G.; Matzger, A. J. *Inorg. Chem.* **2010**, *49*, 5271.
(14) Caskey, S. R.; Wong-Foy, A. G.; Matzger, A. J. *J. Am. Chem. Soc.* **2008**, *130*, 10870.
(15) Porter, W. W.; Wong-Foy, A.; Dailly, A.; Matzger, A. J. *J. Mater. Chem.* **2009**, *19*, 6489.
(16) Hausdorf, S.; Baitalow, F.; Böhle, T.; Rafaja, D.; Mertens, F. O. R. L. *J. Am. Chem. Soc.* **2010**, *132*, 10978.
(17) Wen, L.-L.; Wang, F.; Feng, J.; Lv, K.-L.; Wang, C.-G.; Li, D.-F. *Cryst. Growth Des.* **2009**, *9*, 3581.
(18) Song, Y. J.; Kwak, H.; Lee, Y. M.; Kim, S. H.; Lee, S. H.; Park, B. K.; Jun, J. Y.; Yu, S. M.; Kim, C.; Kim, S.-J.; Kim, Y. *Polyhedron* **2009**, *28*, 1241.
(19) Chui, S. S.-Y.; Lo, S. M. F.; Charmant, J. P. H.; Orpen, A. G.; Williams, I. D. *Science* **1999**, *283*, 1148.
(20) McCoy, M. *Chem. Eng. News* **2010**, *88*, (October 11), 18.
(21) Ahmad, R.; Wong-Foy, A. G.; Matzger, A. J. *Langmuir* **2009**, 11977.
(22) Mueller, U.; Schubert, M.; Teich, F.; Puetter, H.; Schierle-Arndt, K.; Pastré, J. *J. Mater. Chem.* **2006**, *16*, 626.
(23) Czaja, A. U.; Trukhan, N.; Müller, U. *Chem. Soc. Rev.* **2009**, *38*, 1284.
(24) Ameloot, R.; Stappers, L.; Fransaer, J.; Alaerts, L.; Sels, B. F.; De Vos, D. E. *Chem. Mater.* **2009**, *21*, 2580.
(25) Vagin, S. I.; Ott, A. K.; Rieger, B. *Chem. Ing. Tech.* **2007**, *79*, 767.
(26) Lee, Y.-G.; Moon, H. R.; Cheon, Y. E.; Suh, M. P. *Angew. Chem., Int. Ed.* **2008**, *47*, 7741.
(27) Edgar, M.; Mitchell, R.; Slawin, A. M. Z.; Lightfoot, P.; Wright, P. A. *Chem.—Eur. J.* **2001**, *7*, 5168.
(28) Seo, J.; Bonneau, C.; Matsuda, R.; Takata, M.; Kitagawa, S. *J. Am. Chem. Soc.* **2011**, *133*, 9005.
(29) Chen, B.; Liang, C.; Yang, J.; Contreras, D. S.; Clancy, Y. L.; Lobkovsky, E. B.; Yaghi, O. M.; Dai, S. *Angew. Chem., Int. Ed.* **2006**, *45*, 1390.
(30) Fang, Q.-R.; Zhu, G.-S.; Xin, M.-H.; Zhang, D.-L.; Shi, X.; Wu, G.; Tian, G.; Tang, L.-L.; Xue, M.; Qiu, S.-L. *Chem. J. Chin. Univ.—Chin.* **2004**, *25*, 1016.

(31) Charlton, M.; Humberston, J. W. *Positron Physics*; Cambridge University Press: Cambridge, 2001.
(32) Gidley, D. W.; Peng, H. G.; Vallery, R. S. *Ann. Rev. Mater. Res.* **2006**, *36*, 49.
(33) Liu, M.; Wong-Foy, A. G.; Vallery, R. S.; Frieze, W. E.; Schnobrich, J. K.; Gidley, D. W.; Matzger, A. J. *Adv. Mater.* **2010**, *22*, 1598.
(34) Hibbe, F.; Chmelik, C.; Heinke, L.; Pramanik, S.; Li, J.; Ruthven, D. M.; Tzoulaki, D.; Kärger, J. *J. Am. Chem. Soc.* **2011**, *133*, 2804.
(35) Heinke, L.; Kärger, J. *Phys. Rev. Lett.* **2011**, 106.
(36) Tao, S. J. *J. Chem. Phys.* **1972**, *56*, 5499.
(37) Eldrup, M.; Lightbody, D.; Sherwood, J. N. *Chem. Phys.* **1981**, *63*, 51.
(38) Jasińska, B.; Dawidowicz, A. L.; Goworek, T.; Wawryszczuk, J. *Opt. Appl.* **2003**, *33*, 7.
(39) Dull, T. L.; Frieze, W. E.; Gidley, D. W.; Sun, J. N.; Yee, A. F. *J. Phys. Chem. B* **2001**, *105*, 4657.
(40) Koh, K.; Wong-Foy, A. G.; Matzger, A. J. *Chem. Commun.* **2009**, 6162.
(41) Yoo, Y.; Jeong, H.-K. *Cryst. Growth Des.* **2010**, *10*, 1283.
(42) The surface barrier phenomenon has been investigated previously in zeolites (for example, Micke, A.; Bülow, M.; Kočiřík, M. *J. Phys. Chem.* **1994**, *98*, 924–929) and very recently in a model MCP (see refs 34 and 35). In the more recent studies, the surface was characterized as having a heterogeneous mixture of completely blocked (zero-permeability) and completely open (infinite permeability) sites. A logical extension of this concept may be applicable to our material, where the surface is characterized solely by sites of zero-permeability. This contrasts with earlier work since pore blockage in Zn-HKUST-1 is found to be complete by gas sorption experiments.
(43) Maes, M.; Vermoortele, F.; Alaerts, L.; Couck, S.; Kirschhock, C. E. A.; Denayer, J. F. M.; De Vos, D. E. *J. Am. Chem. Soc.* **2010**, *132*, 15277.
(44) Ameloot, R.; Liekens, A.; Alaerts, L.; Maes, M.; Galarneau, A.; Coq, B.; Desmet, G.; Sels, B. F.; Denayer, J. F. M.; De Vos, D. E. *Eur. J. Inorg. Chem.* **2010**, 3735.
(45) Park, T. H.; Cychosz, K. A.; Wong-Foy, A. G.; Dailly, A.; Matzger, A. J. *Chem. Commun.* **2011**, *47*, 1452.